Journal of Power Sources 448 (2020) 227258

Contents lists available at ScienceDirect

Journal of Power Sources

journal homepage: www.elsevier.com/locate/jpowsour

A regenerative braking system for internal combustion engine vehicles using supercapacitors as energy storage elements - Part 2: Simulation results

Emiliano Pipitone [a], Gianpaolo Vitale [b,*]

[a] Department of Engineering, University of Palermo, Italy
[b] ICAR, Institute for High Performance Computing and Networking, National Research Council of Italy, Italy

GRAPHICAL ABSTRACT

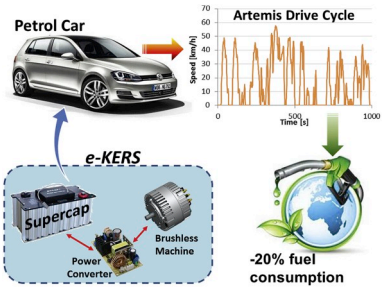

ARTICLE INFO

Keywords:
Kinetic energy recovery system
Supercapacitor
Ultracapacitor
Vehicle fuel economy
Regenerative braking
Urban driving cycle
Hybrid vehicle

ABSTRACT

In this two-part work, an electric kinetic energy recovery system (e-KERS) for internal combustion engine vehicle (ICEV) is presented and its performance evaluated through numerical simulations. The KERS proposed is based on the use of a supercapacitor as energy storage, interfaced to a brushless machine through a properly designed power converter. In Part 1, the system is described and analysed, and the mathematical model used for the simulations is presented. For each component of the KERS, the real efficiency and the power or energy limitations are adequately considered. In Part 2, the energetic and economic advantages attainable by the proposed KERS are evaluated using MATLAB Simulink, considering a widely diffused passenger car and two reference driving cycles (ECE-15 and Artemis urban). Energy savings of the order of 20% were found, with a slight increase in vehicle weight (+2%) and with an overall commercial cost that would be compensated in 5 years thanks to the fuel economy improvement, to which corresponds an equal reduction of CO_2 emissions. The low complexity of the system, never proposed for ICEV, the moderate weight of its components, and their availability on the market, make the solution presented ready for the introduction in current vehicle production.

1. Introduction

In the first part of this two-papers work [1] the authors presented and described an electric kinetic energy recovery system (e-KERS) for internal combustion engine vehicles (ICEV), schematically represented in Fig. 1 together with the vehicle drivetrain. The supercapacitors bank

* Corresponding author.
E-mail address: gianpaolo.vitale@icar.cnr.it (G. Vitale).

https://doi.org/10.1016/j.jpowsour.2019.227258
Received 24 June 2019; Received in revised form 9 September 2019; Accepted 2 October 2019
Available online 23 October 2019

(SC) is the unique energy storage of the system and is electrically interfaced, by means of an expressly designed power converter (PC), to a motor-generator unit (MGU). The MGU is mechanically connected to the drive shaft via a fixed gear ratio and converts the vehicle kinetic energy into electric energy and vice versa. The system was conceived to recover the vehicle kinetic energy during braking phases by charging the supercapacitor, whose stored energy is employed by the MGU for successive vehicle acceleration thus lowering the power demand to the thermal engine. It gives advantages in terms of reduced fuel consumption and air pollution. In the Part 1, the authors also presented a mathematical model developed for the evaluation of the performance provided by the proposed e-KERS through numerical simulations; for each component of the KERS, the model adequately takes into consideration the real efficiency as well as the power or energy limitations.

The purpose of this second part paper is to evaluate the energetic performances and economic advantages connected to the implementation of the proposed KERS in a passenger car. In effect, the use of a SC as single energy storage element has been proposed only when large spaces and weight were allowed, as for example in the case of electric city rail [2] or hybrid city bus [3], where energy savings of about 40% were obtained. In the present study, instead, the authors aim to evaluate the plausible reduction of fuel consumption, and related CO_2 emissions, that could be achieved by the implementation of the electric KERS proposed in traditional passenger cars endowed of internal combustion engines (ICE), with the aim to improve their sustainability and environmental compatibility. The system studied in this paper may contribute to their hybridization process of ICEV, already started with the development of the so-called starter-generators system [4], whose growth in power, control complexity and launching ability could further promote the use of supercapacitors as energy storage elements for KERS application.

2. KERS sizing

The effectiveness of the KERS proposed in reducing the vehicle energy demand was evaluated considering one of the most diffused passenger car in Europe [5], whose main characteristics are reported in Table 1.

As it can be noted, the vehicle is characterized by a 1.4 L gasoline fuelled engine and by a reference mass (i.e. including fuel, with an addition of 100 kg to account for driver and luggage, as prescribed by EU directive 95/48) of 1315 kg, which are average values in the typical range for passenger cars employed in urban context. Table 2 reports the fuel consumption and CO_2 emissions experimentally measured on the considered vehicle [6] with regards to two different standard driving cycles: the ECE-15 and the Artemis urban. Standard driving cycles are the type approval test carried out to evaluate the air pollution and fuel consumption of vehicles equipped with internal combustion engines. The procedure consists in reproducing on a roller test bench a typical vehicle speed profile as function of time, with the aim to simulate the vehicle usage both in the urban and in the extra-urban area and to measure the resulting air pollution and fuel consumption. There are

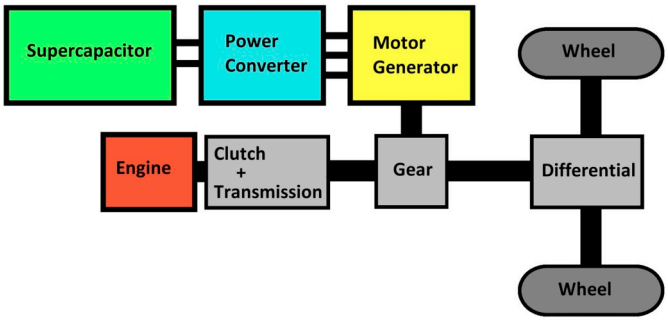

Fig. 1. Drivetrain layout of the vehicle with KERS.

Table 1
Characteristic parameters of the vehicle considered in this study.

Brand and model	Volkswagen Golf 1.4 TSI
Segment	C – Medium cars
Reference mass [kg]	1315
Engine displacement [L]	1.39
Maximum output power [kW]	90
Homologation	Euro 5
Drag coefficient c_x	0.280
Frontal surface area [m^2]	2.63
Fuel	Gasoline
Fuel LHV [MJ kg^{-1}]	43.4
Fuel density [kg m^{-3}]	730
Tyres	205/55R16
Wheel radius [m]	0.316
Differential gear ratio τ_D	3.65

Table 2
Measured energy consumption and CO_2 emissions on both driving cycles considered [6].

	ECE-15	Artemis urban
Cycle length [km]	0.995	4.87
Fuel consumption [L (100 km)$^{-1}$]	8.30	10.3
CO_2 emissions [g km^{-1}]	193	239

several commonly used driving test cycles all over the world [7,8]. For more than 20 years the European union adopted the so called *new European driving cycle* (NEDC). It is composed of four repetitions of the ECE-15, used to simulate vehicle use in the urban area (also known as UDC, i.e. urban driving cycle), and a single repetition of the *extra-urban driving cycle* (EUDC), which instead was dedicated to the extra-urban use of the vehicle. The mentioned European driving cycle was however considered unable to reproduce the real vehicle use, above all in the urban conditions [7,8], because of the few (and too mild) transient phases which compose the cycles. This led to the study and development of alternative driving cycles, more representative of the real vehicle use, such as the ARTEMIS cycle [9], which is also divided into urban, road and motorway parts, and the more recent *worldwide harmonized light vehicles test cycles* (WLTC), which, after the transition phase covering the years 2017–2019, will definitively replace the NEDC cycle in all the UNECE member states for vehicle test approval [10]. Since a kinetic energy recovery system reveals effective only in urban application, where the vehicle accelerations may be obtained by exploiting the energy recovered during the braking phases, the authors focused on the urban driving cycles for the design of the KERS and for the evaluation of its performances. Based on the availability of measured fuel consumption data [6], the European ECE-15 driving cycle and the Artemis urban driving cycle, reproduced in Fig. 2, were taken into consideration.

Obviously, each KERS component must be able to manage the power connected to the transient vehicle phases (acceleration or braking phases), and this means that the speed of variation of the vehicle kinetic energy constitutes a constraints for the power sizing of each KERS element. Furthermore, the storage capacity of the supercapacitor should be able to face up the vehicle kinetic energy variation adequately. The kinetic energy recovery system must hence fulfil two separate conditions: the first regards the maximum energy that can be stored or supplied, and the second regards the maximum power to be managed. These two constraints bind the design of the power conversion chain, i.e. the size of each element of the KERS.

As regards the first condition required for KERS sizing, i.e. the maximum storable energy, the authors considered that the supercapacitor cannot supply to the MGU energy that has not been previously stored during previous braking phases. According to this observation, the authors determined the maximum storable energy on the basis of the braking phases of the driving cycle, ignoring, for the purpose, the acceleration phases.

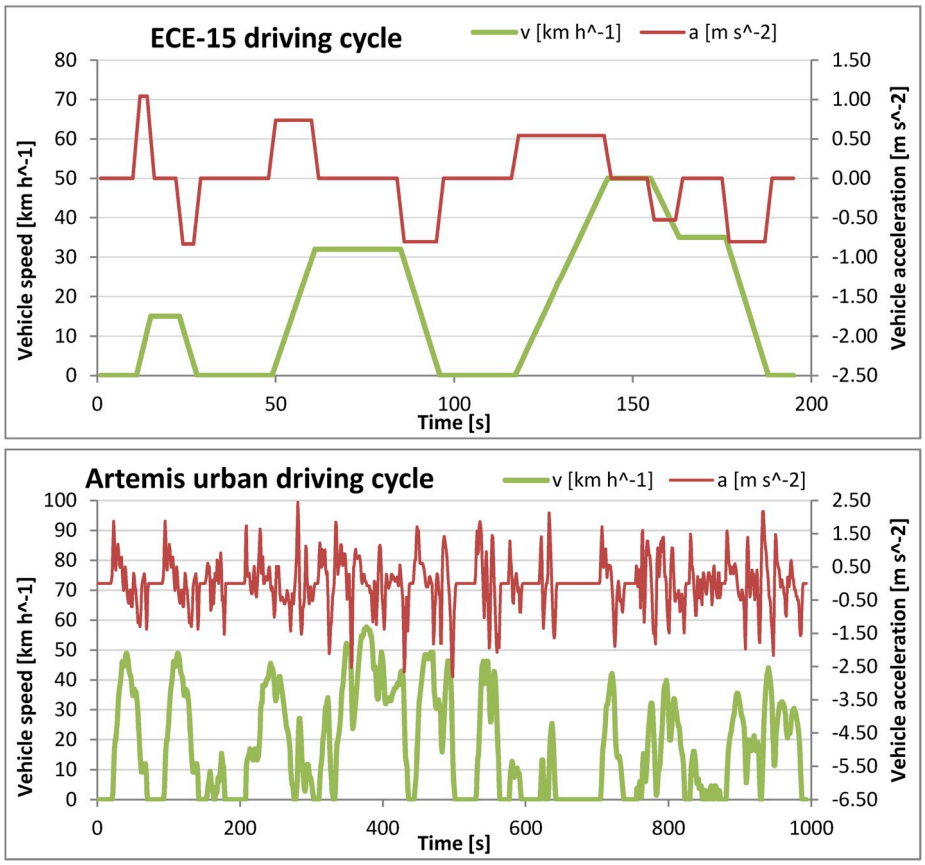

Fig. 2. Speed and acceleration profile of the ECE-15 cycle (upper) and Artemis urban cycle (lower).

Neglecting, for the moment, the efficiency of the KERS components, the total amount of energy E_{br} that could be recovered during a braking phase can be estimated by the integration of the braking power P_{br}, which, in turn, as already observed in equation (11) of Part 1, is linked to the *road load* power P_{road} and to the inertial power $m_v \cdot a \cdot v$; it results that:

$$E_{br} = \int_{braking} P_{br}(t)\ dt = \int_{braking} [-P_{road}(t) - m_v \cdot a(t) \cdot v(t)]\ dt \quad (1)$$

It is worth to point out that two or more successive braking phases, without intermediate acceleration phases, allow storing the sum of the energy recovered by each single phase. The recoverable energy was then evaluated for the vehicle considered on both ECE-15 and Artemis urban driving cycles, as reported in Fig. 3.

The resulting values of the maximum storable energy are reported in Table 3: as it can be observed, for the vehicle considered, the required capacity of the energy storage should be around 100 kJ, apart from the urban driving cycle adopted: this is quite an interesting result, since establishes a sort of equivalence between ECE-15 and Artemis urban driving cycles. Two factors must be, however, still considered:

1. As mentioned, the evaluation carried out does not take into account the energy conversion efficiencies of the real components of the KERS, which will instead properly considered further on in the simulations, once the KERS components have been selected.
2. As shown in the description of the Simulink model, the minimum working voltage of the SC has been assumed to correspond to 40% of rated storable energy: the supercapacitor hence can exploit only 60% of its nominal capacity.

In consideration of both factors, the author increased by 80% the minimum required energy storage capacity, which was hence assumed to be at least 180 kJ.

As regards the second constraint, the rated power of each KERS components should be related to the inertial power P_I required during the accelerations and to the recoverable power P_{br} during the braking phases of the vehicle, both reported, for the vehicle considered, in Fig. 4 for the ECE-15 and for the Artemis urban cycle. As it can be noted, differently from the maximum recoverable energy, the two urban cycles show noticeable differences in terms of maximum power values. As summarized in Table 3, according to the Artemis urban cycle, the KERS should manage the power of 34.9 kW, while 12.7 kW would be sufficient if the ECE-15 cycle is considered.

Based on the substantial difference between the power requirements emerged by the two urban cycles, the authors decided to consider four KERS of different power sizes, in order to determine, through simulations, the optimal choice.

Table 3 also shows the mean values of the power that the KERS should manage, evaluated considering the inertial power P_I and the recoverable power P_{br} during the whole driving cycle: as it can be noted, this time the two urban driving cycles produce similar results.

The design of the KERS proposed in this work was carried out considering solutions with the minimum impact on the vehicle weight, focusing on products already available on the market, which also allowed to evaluate the related costs. Given the minimum energy requirements determined in the previous section (i.e. 180 kJ), the authors selected the supercapacitor Green Tech GTSM-48V165FUS, whose main characteristics [11] and commercial cost are reported in Table 4. As shown, the energy storable by this supercapacitor amply satisfies the requirement. As regards the power output, the supercapacitor datasheet reports a maximum allowed current of 2275 A, which, at the rated voltage of 48 V, means a maximum allowed power of 109 kW, which is quite above the highest power requirement (35 kW in Table 3).

It must be pointed out, however, that the real maximum available

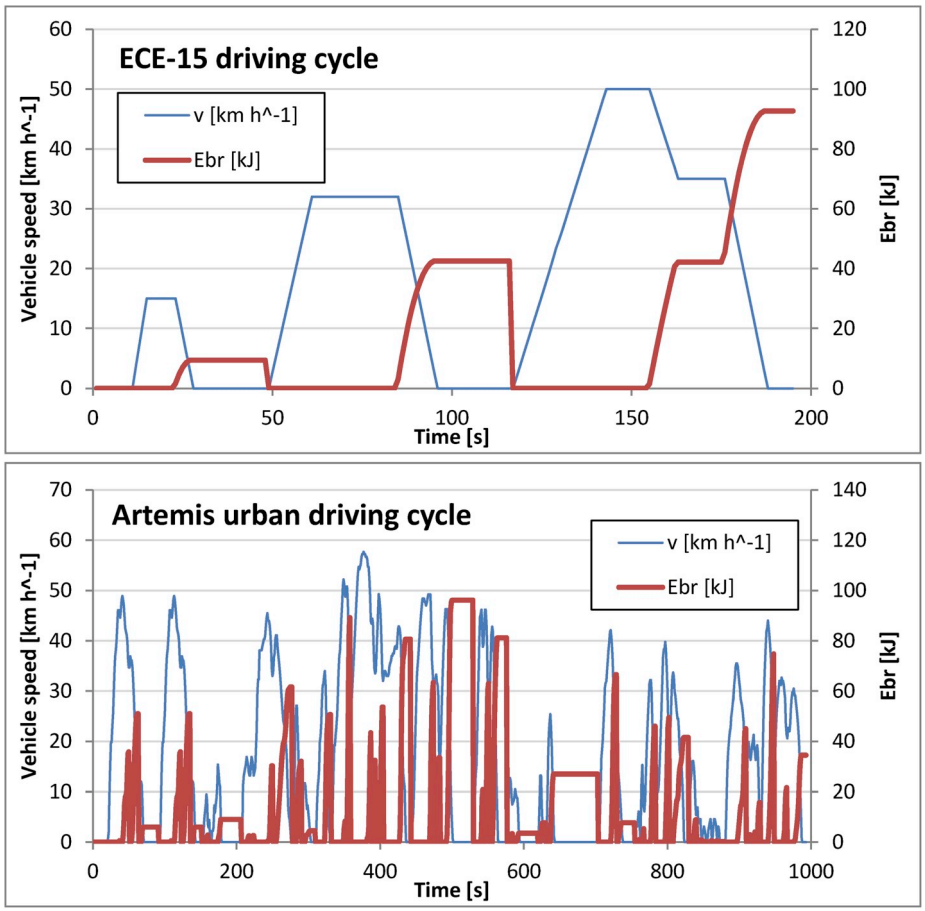

Fig. 3. Energy recoverable E_{br} in the braking phases of the ECE-15 cycle (upper) and of the Artemis urban cycle (lower).

Table 3
Maximum KERS power and maximum recoverable energy evaluated on both ECE-15 and Artemis urban cycles (for the vehicle considered in Table 1).

Maximum recoverable energy [kJ]		Maximum transient power [kW]		Mean transient power [kW]	
ECE-15	Artemis urban	ECE-15	Artemis urban	ECE-15	Artemis urban
92.7	96.2	12.7	34.9	4.26	5.24

power of the supercapacitor is

$$P_{SC,max}(t) = V_{SC}(t) \cdot i_{PC,max} \quad (2)$$

and depends on the instantaneous working voltage $V_{SC}(t)$ of the supercapacitor, which continuously varies during KERS operation together with the amount of energy stored, and on the maximum current allowed in the power converter $i_{PC,max}$, which, as shown further on, will be properly determined to meet the power requirement.

As regards the motor-generator units, the authors focused on compact, open frame, fan-cooled three phases brushless motors, which are available on the market with adequate power size [12,13]. According to the range of output power identified in the previous section (from 12.7 kW to 34.9 kW, as reported in Table 3) the authors selected the four products listed in Table 5.

As it can be observed, the selected motors can deliver, for a period not exceeding 30 s, peak powers from 11 to 30 kW (involving the related peak current levels), which comply with the requirements, even if the allowed continuous power levels are 2.4–3 times lower: this is a fundamental feature, since allows the selected machines to fulfil the transient vehicle phases (usually shorter than 30 s), while maintaining the reasonable weights and costs of low power machines. The maximum torque $T_{MGU,\ stall}$ that can be delivered as a motor (or received as a generator) without causing overheating or demagnetization of the permanent magnets, ranges from 38 to 81 Nm. As already pointed out in paper Part 1, this kind of brushless motor needs a proper controller (which, in the system proposed, is embedded into the power converter of Fig. 1) to transforms DC into AC power and supply the motor with proper sinusoidal waveforms. Moreover, as already stated, the brushless motor is assumed to be current-controlled, i.e. the torque delivered (or received) is modulated through the control of the phase-currents, as described in Ref. [14]: this task is obviously accomplished by the power converter, which was expressly designed for the purpose [15]. The maximum speed of revolution of all the selected motors does not allow a direct connection with the drive shaft, making hence necessary the adoption of a gear drive, whose efficiency η_G (supposed 0.97 in this paper) will certainly condition the overall KERS efficiency and will be taken into account in the numerical simulations. With a suitable optimized design, the MGU could be coaxial with drive shaft, eliminating hence the necessity of a gear and increasing the overall KERS efficiency. As already mentioned in Part 1 of this paper, the brushless gear ratio τ_G was fixed considering to reach the maximum motor rotation speed at the vehicle speed of 60 km h^{-1}.

Once the supercapacitor and the motor-generator units are selected, the power converter of each KERS can be adequately sized to manage the power transfer during both acceleration and braking transients. Considering the structure of the proposed KERS (see Fig. 1), the power flux involving each element is schematically reported in Fig. 5 both for an acceleration and for a braking phase. This diagram helps to identify the magnitude of the power managed by each component of the KERS,

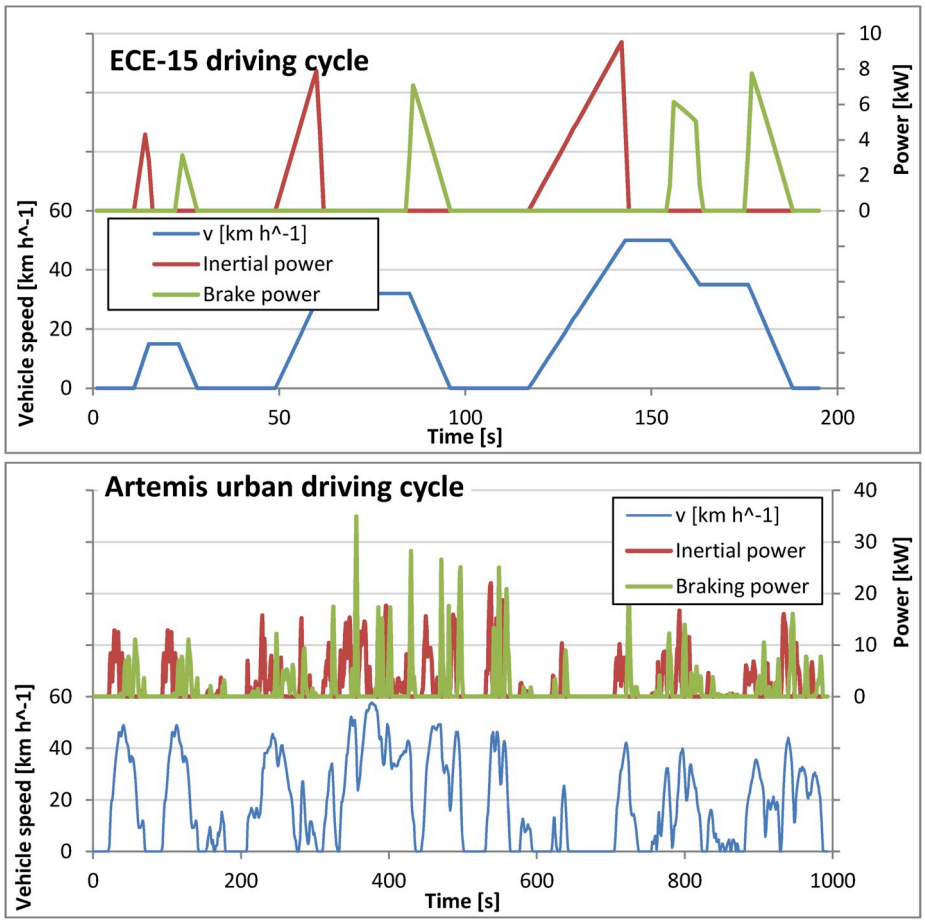

Fig. 4. Inertial power P_I and braking power P_{br} in the ECE-15 cycle (upper) and in the Artemis urban cycle (lower).

Table 4
Supercapacitor selected from the available product on the market [11].

Brand	Green Tech
Model	GTSM-48V165FUS
Capacitance C [F]	165
Rated voltage $V_{SC,max}$ [V]	48
Storable energy $E_{SC,max}$ [kJ]	190.1
Maximum peak current [A]	2275
Maximum continuous current [A]	100
ESR [mΩ]	5.00
Weight [kg]	14.5
Commercial cost [€]	602

Table 5
Motor generator units selected from the available products on the market [12, 13].

Brand	MOTENERGY			
Model	ME1305	ME1117	ME1114	ME1115
Max DC voltage $V_{MGU,max}$ [V]	72	72	72	96
Continuous motor power [kW]	4.40	4.40	10.0	12.0
Continuous input DC current [A]	80	80	180	180
Peak motor power [kW]	11.0	14.0	24.0	30.0
Peak DC current $i_{MGU,max}$ [A]	230	300	600	600
Peak stall torque $T_{MGU,\ stall}$ [Nm]	38.0	38.0	65.1	81.3
Max speed $n_{MGU,max}$ [rpm]	5000	5000	5000	5000
Weight [kg]	10.0	10.0	15.9	15.9
Rotor inertia [kg cm^2]	52.0	52.0	45.0	45.0
Max Efficiency	0.90	0.90	0.92	0.92
Commercial cost [€]	527	544	606	606

such as the power converter. It is worth to point out that the efficiency of each component involved in the power transfer from the wheels to the supercapacitor (and vice versa) is taken into account in the diagram of Fig. 5, including the efficiency η_G of the brushless gear, and the efficiency of the final differential gear η_D.

As shown in Fig. 5, during vehicle acceleration, the PC should be able to deliver the power (P_{MGU}/η_{MGU}) to the MGU, while during a braking phase the PC should transmit the power ($P_{MGU} \cdot \eta_{PC}$) to the supercapacitor, being η_{PC} and η_{MGU} the efficiency of the power converter and of the MGU respectively. It is hence clear that the power converter will manage the maximum power levels during the acceleration process, and its maximum output power $P_{PC,max}$ is determined by the maximum input power to the MGU, which, in turns, depends on the maximum allowed current and voltage on the DC side of the MGU controller:

$$P_{PC,\max} = V_{MGU,\max} \cdot i_{MGU,\max} \tag{3}$$

The data reported in Table 5 allow to determine the maximum output power $P_{PC,max}$ of the power converter, for each brushless machine considered. As already shown in Fig. 3 of Part 1 of this paper, the efficiency curve of such a power converter [15] reveals that for power exceeding 10% of the maximum, the efficiency remains at its best value, i.e. 0.93.

The maximum allowed DC current in the power converter $i_{PC,max}$ was determined on the basis of two considerations:

(1) as already mentioned, the vehicle acceleration phases involve the highest power levels in the power converter; as clear from the power fluxes in Fig. 5, during vehicle acceleration the PC deliver the power (P_{MGU}/η_{MGU}) to the MGU, receiving the power ($P_{MGU}/(\eta_{MGU} \cdot \eta_{PC})$) from the supercapacitor.

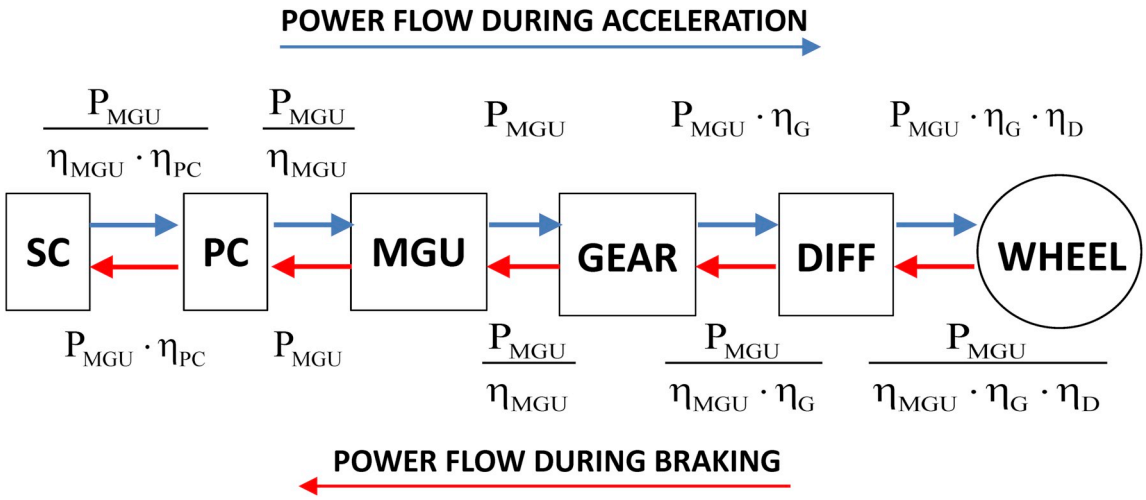

Fig. 5. Schematic representation of the KERS power fluxes in both acceleration and braking phase.

(2) the PC works on two different voltage levels: on one side, it exchanges power with the supercapacitor, whose working voltage $V_{SC}(t)$ depends on the amount of energy stored and may reach the maximum value $V_{SC,max}$ (48 V for the model considered, as reported in Table 4); on the other side, the PC exchanges power with the MGU, which, in this work, is supposed to work always at its maximum voltage level $V_{MGU,max}$ (from 72 to 96 V, as reported in Table 5) with the aim to maintain as low as possible the current involved and the related losses.

It results that, for the power converter of the considered system, the working current on the supercapacitor side is always higher than the current on the DC side of the MGU:

$$i_{SC}(t) = \frac{P_{MGU}(t)}{\eta_{MGU}(t)\cdot\eta_{PC}(t)\cdot V_{SC}(t)} > \frac{P_{MGU}(t)}{\eta_{MGU}(t)\cdot V_{MGU,\max}} = i_{MGU}(t) \tag{4}$$

Hence the power converter of each KERS was sized to manage the maximum allowed current:

$$i_{PC,\max} = \frac{P_{PC,in,\max}}{V_{SC,\max}} = \frac{P_{PC,\max}}{\eta^*_{PC}\cdot V_{SC,\max}} = \frac{P_{MGU,\text{in},\max}}{\eta^*_{PC}\cdot V_{SC,\max}} \tag{5}$$

being $P_{PC,in,max}$ the maximum input power to the power converter, evaluated through its efficiency at the maximum output power η_{PC}* (0.93, as shown in Fig. 3 of Part 1). Summing up, the specifications of the power converters of each KERS considered in this work are reported in Table 6. It is worth to point out that the maximum allowed current determined for each power converter is lower than the maximum current allowed by the supercapacitor (2275 A in Table 4) and put a limit to the power that the supercapacitor can delivered to the MGU, as will be pointed out in the description of the simulation model. On the other hand, it would not be appropriate to size each PC on the same maximum current (and maximum power) of the supercapacitor, since the high cost increment would not be counterbalanced by an efficiency improvement of the whole KERS: the power limits imposed by each MGU, in effect, would cause the PC to work with too low power and hence, as shown in Fig. 3 of Part 1, with low efficiency. The cost and the weight of each power converter was estimated on the basis of its component [15] and is also reported in Table 6.

Summing the weights and the costs of all the components of each KERS configuration, the overall commercial cost and weight of the four KERS assembly is obtained and reported in Table 7; the same table also reports the overall weight increment caused to the vehicle mass by the implementation of the KERS: as it can be observed, the increment ranges from 2% to 3%, which is considered a reasonable value.

Table 6
Power converter specifications for each of the four KERS considered.

	KERS1	KERS2	KERS3	KERS4
Peak motor power [kW]	11.0	14.0	24.0	30.0
Max output power $P_{PC,max}$ [kW]	16.56	21.60	43.20	57.60
Max current $i_{PC,max}$ [A]	371	484	968	1290
Max efficiency	0.930	0.930	0.930	0.930
Max input power $P_{PC,in,max}$ [kW]	17.8	23.2	46.5	61.9
Weight [kg]	2.30	3.00	6.00	8.00
Commercial cost [€]	360	469	938	1251

3. Performance parameters and probability indexes

This section presents the performance parameters and indexes taken into consideration for the evaluation of the energetic and economic advantages connected to the implementation of the e-KERS proposed. Starting from the original vehicle, i.e. without KERS contribution, it is obvious that the traction power P_{trac} necessary for vehicle propulsion is completely delivered by the thermal engine:

$$P_{trac}(t) = P_I(t) + P_{road}(t) = P_{eng}(t)\cdot\eta_T\cdot\eta_D \tag{6}$$

where P_I ($= m_v\cdot a\cdot v$) is the *inertial power*, i.e. the power required by inertia force, P_{eng} is the power delivered by the internal combustion engine, while η_T and η_D represent the efficiency of the main transmission and of the final differential gear respectively.

Given the vehicle speed profile as function of time, the total amount of energy E_0 produced by the thermal engine to perform a complete driving cycle without KERS is hence:

$$E_0 = \int_{cycle} P_{eng}(t)\cdot dt = \int_{cycle} \frac{P_{trac}(t)}{\eta_D\cdot\eta_T}\, dt \tag{7}$$

In this evaluation no energy recovery is performed during the braking phases (the original vehicle is considered); moreover, being related to the vehicle dynamics only, it does not involve the engine efficiency, and hence does not represent the real energy consumption of

Table 7
Overall cost and weight of the four KERS considered.

	KERS1	KERS2	KERS3	KERS4
Peak motor power [kW]	11.0	14.0	24.0	30.0
Commercial cost [€]	1488	1615	2146	2459
Weight [kg]	26.8	27.5	36.4	38.4
Weight increment [%]	2.0%	2.1%	2.8%	2.9%

the vehicle, which will be considered further on.

When considering the application of the KERS proposed, the driving cycle simulations were performed including the KERS mass into the vehicle mass; moreover, with the aim to nullify the effect of the initial energy content E_i of the SC, each driving cycle simulation involving the use of the KERS was iteratively repeated assuming that the energy stored in the supercapacitor at the beginning of the cycle was equal to the energy content evaluated at the end of the previous cycle simulation: the iteration was stopped when the difference between these two values resulted lower than 10 J (negligible with respect to the nominal energy of the SC, i.e. 190 kJ); this procedure allowed to obtain results nearer to the real use of the vehicle on distances much longer than that of the driving cycle (0.995 km and 4.87 km for the ECE-15 and Artemis urban respectively, as reported in Table 2)

The advantage connected to the use of the KERS was evaluated considering that, as already stated by equation (12) of Part 1, in the system proposed (Fig. 1) the power produced by the brushless motor P_{MGU}, reduced by the MGU gear efficiency η_G, contributes to vehicle acceleration reducing the power traction demand to the thermal engine:

$$P_{trac}(t) = P_I(t) + P_{road}(t) = \left[P_{MGU}(t)\cdot\eta_G + P_{eng}(t)\cdot\eta_T\right]\cdot\eta_D \tag{8}$$

According to this observation, the traction energy E_S delivered by the KERS during a driving cycle is computed as:

$$E_S = \int_{P_{MGU}>0} P_{MGU}(t)\cdot\eta_G\cdot\eta_D\cdot dt \tag{9}$$

being the brushless motor power $P_{MGU}(t)$ evaluated by equations (27) and (39) of the model (entirely presented in the Part 1 of this paper). As indicated, this integral is restricted to the acceleration phases only, when the power delivered by the brushless motor $P_{MGU}(t)$ is positive. It results that, for the vehicle equipped with the proposed KERS, the amount of energy produced by the thermal engine to perform a complete driving cycle E_K is hence reduced to:

$$E_K = \frac{1}{\eta_D\cdot\eta_T}\left[\int_{cycle} P_{trac}(t)\cdot dt - E_S\right] = \frac{1}{\eta_D\cdot\eta_T}\int_{cycle}\left[P_I(t)+P_{road}(t)\right]\cdot dt - \frac{E_S}{\eta_D\cdot\eta_T} \tag{10}$$

It is worth noting that the integral of equation (10) differs from the integral of equation (7) because of the KERS mass added to the vehicle mass.

Since the difference E_O-E_K represents the reduction of the energy demand to the thermal engine, the **net energy saving ε_K** was evaluated as:

$$\varepsilon_K = \frac{E_O - E_K}{E_O} = 1 - \frac{E_K}{E_O} \tag{11}$$

The energy recovery effectiveness of the proposed system was evaluated comparing the traction energy reduction E_S obtained by the KERS implementation, with the maximum energy E_{MR} that could be ideally recovered during a whole driving cycle, evaluated as:

$$E_{MR} = \int_{cycle} P_{br}(t)\ dt \tag{12}$$

being the braking power $P_{br}(t)$ evaluated by equation (11) reported in Part 1 of the paper. As obvious, this integral takes into account the braking phases only, i.e. the only phases during which a KERS can recover the vehicle kinetic energy.

The **recovering efficiency η_K** of the KERS was hence evaluated as:

$$\eta_K = \frac{E_S}{E_{MR}} \tag{13}$$

A further characterization of the proposed KERS was carried out by the authors taking into account two indexes frequently employed in the analysis of energy systems reliability, i.e. the *Loss of Load Probability* (LOLP) and the *Loss of Energy Probability* (LOEP).

A loss of load (or power) may occur during both an acceleration and a braking phase. In the first case, a loss of load occurs if the required inertial power P_I is higher than the maximum power that the brushless motor can deliver $P_{MGU,max}$. Assuming $p_L(t)$ to be the Boolean variable which determines if a loss of load is verified or not (i.e. $p_L(t) = 1$ or $p_L(t) = 0$ respectively), during an acceleration phase (i.e. $a(t) > 0$):

$$p_L(t) = 1 \quad \text{if} \quad \frac{P_I(t)}{\eta_G\cdot\eta_D} > P_{MGU,\max}(t) \tag{14}$$

being the maximum MGU output power evaluated through model equation (24) (Part 1). If the inequality in equation (14) is not true, the loss of load is not verified and $p_L(t) = 0$.

In a braking phase (i.e. $P_{br}(t) > 0$), instead, a loss of load occurs if the braking power involves a too high input power for the generator (or for the supercapacitor); in a braking phase hence

$$p_L(t) = 1 \quad \text{if} \quad P_{br}(t)\cdot\eta_G > P_{MGU,\text{in},\max}(t) \tag{15}$$

where the maximum input power to the MGU $P_{MGU,in,max}(t)$ is evaluated by the model equation (46). As before, if the inequality in equation (15) is not verified, no loss of load occurs and $p_L(t) = 0$.

Since the LOLP index expresses the probability that the MGU or the supercapacitor will not allow a sufficient power exchange, it can be easily evaluated on the basis of the Boolean variable $p_L(t)$:

$$LOLP = \frac{\int_{cycle} p_L(t)\ dt}{\int_{cycle} dt} = \frac{\int_{cycle} p_L(t)\ dt}{\Delta t_{cycle}} \tag{16}$$

where Δt_{cycle} denotes the whole cycle duration.

The *Loss of Energy Probability* (LOEP) index is similar to the LOLP, with the difference that it is focused on the energy exchanged between the storage system and the MGU. The interest is now on the capability of the storage system to serve the MGU both in the acceleration and in the braking phases. In the KERS considered in this work, a loss of energy will occur during an acceleration phase (i.e. $a(t) > 0$) if the supercapacitor reaches the minimum energy content $E_{SC,min}$ (see model equation (38)), thus becoming unable to further supply the MGU (as therefore represented by the model equation (39)); for the same KERS, a loss of energy will also occur if, during a braking phase ($P_{br}(t) > 0$), the supercapacitor reaches its maximum storable energy $E_{SC,max}$ (see model equation (55)), thus becoming unable to store any extra energy that the MGU could provide (as stated by the model equation (56)).

Assuming hence the Boolean variable $p_E(t)$ to determines if a loss of energy is verified or not (i.e. $p_E(t) = 1$ or $p_E(t) = 0$ respectively), for the KERS considered is:

$$p_E(t) = 1 \ \text{ if } \begin{cases} E_{SC}(t) = E_{SC,\min} \quad \text{AND} \quad a(t) > 0 \\ E_{SC}(t) = E_{SC,\max} \quad \text{AND} \quad P_{br}(t) > 0 \end{cases} \tag{17}$$

If the conditions expressed in equation (17) are not true, the loss of energy is not verified and $p_E(t) = 0$.

With the same meaning of the symbols, the LOEP index can be hence evaluated as:

$$LOEP = \frac{\int_{cycle} p_E(t)\ dt}{\int_{cycle} dt} = \frac{\int_{cycle} p_E(t)\ dt}{\Delta t_{cycle}} \tag{18}$$

The closer to zero the value of these indexes are, the lower is the probability that the KERS elements cannot exchange the necessary power or energy. In principle, the best value of both performance indexes is zero, but this would imply the adoption of too expensive and heavy storage system or MGU. Due to the two limiting factors weight

and cost, the element of the KERS will not allow to store all the energy (or to transfer all the power) required by the vehicle during a braking phase, and will not allow to transfer all the energy (or deliver all the power) required for the acceleration phases. For this reason, not all transients will be satisfied by the selected components, and the performance indexes will give an idea of the suitability of the design performed: a low value of the indexes of probability will ensure that the energy (or the power) is adequately managed in most cases, without weighing down the vehicle and with reasonable costs.

4. Simulation results and discussions

As mentioned before, the model presented in Part 1 of this paper was employed in numerical simulations performed using MATLAB Simulink to evaluate the energetic and economic benefit attainable by the implementation of the proposed e-KERS. To this purpose, the vehicle specified in Table 1 was considered to follow the speed-time profiles of both driving cycles adopted. Table 8 reports the model configuration parameters adopted in the simulation performed.

An example of the simulation output is given in the following figures, obtained considering the implementation of the KERS2 (i.e. with peak motor power of 14 kW). The upper graph of Fig. 6 reproduces the vehicle speed and acceleration during a time interval of 40 s of the Artemis urban cycle, while the lower graph reports the energy content of the supercapacitor together with the progress of the two Boolean variables p_L and p_E related to the probability indexes LOLP and LOEP respectively. With reference to the same time interval, the upper-left graph in Fig. 7 shows the progress of the inertial power required by vehicle acceleration, together with the actual and the maximum MGU output power (KERS2): it can be noted that, due to the limitations described in the model equations (19) to (24) (Part 1 of this paper), the MGU is unable to follow the inertial power required by vehicle acceleration.

The same upper-left graph of Fig. 7 also shows that, when the energy content of the SC reaches the minimum level $E_{SC,min}$ (as reported in the lower graph of Fig. 6), the MGU output power becomes null, as prescribed by the model equation (39). The upper-right graph in Fig. 7 instead reports the braking power required by the vehicle, together with the actual and the maximum input power to the brushless generator during the braking phases of the same time interval. As it can be observed, the already mentioned limitations cut the power that the MGU can manage, making the maximum allowed input power significantly lower than the required braking power. The two lower graphs in Fig. 7 show, for the same time interval, the comparison between the power required by the vehicle (inertial or braking), the actual power transferred by the SC (output or input) and its maximum manageable power, which, as already mentioned, depends on the amount of energy stored: as it is evident, in most of the cases, the power transferred by the SC results lower than its maximum allowed power, pointing out hence that the limits imposed by the selected MGU are the main responsible of the incapability of the e-KERS to satisfy the power demand during vehicle transients completely. The Boolean variables reported in the lower graph of Fig. 6 show that a loss of load ($p_L = 1$) is recognized whenever the brushless machine is unable to satisfy the necessary inertial power (acceleration phases) or the required braking power (braking phases); as regards the loss of energy (i.e. $p_E = 1$), it can be noted that, in the considered time interval, this condition occurred only when the stored energy reached the minimum level.

The upper graph in Fig. 8 reports the current flowing through the DC side of the MGU controller during the Artemis urban cycle performed with KERS2; it can be observed that, despite the high spikes, the RMS value remains well below the allowed continuous current exposed in Table 5: this confirms the suitability of the selected brushless machines, which, as already pointed out, can support peak power level from 2.4 to 3 times higher the continuous power level.

The lower graph of Fig. 8 reports the current flowing on the supercapacitor side instead: as it can be noted, the peaks remain well below the allowed peak current (reported in Table 4), while the RMS current reaches the allowed continuous level (see Table 4).

The overall results of the simulations performed on the ECE-15 driving cycle considering the four different KERS combination are reported in Table 9: as it can be observed, the e-KERS proposed revealed very effective, with recovery efficiency between 48% and 54%, and energy saving between 16% and 19%. The increase of the MGU power size did not produce an advantage, since both energetic parameters significantly decreased moving from smaller to larger machines: the mild transient phases of the ECE-15 cycle could not exploit the higher power size, which instead caused both the supercapacitor and power converter to work with low power and hence with low efficiencies.

The probability indexes revealed low values, confirming hence the suitability of component selected for the KERS assembly; increasing the power size reduced the probability that the KERS could not satisfy the power requirement of the transient vehicle phases, thus causing a sharp decrease of the LOLP index, which became null with KERS3 and KERS4. At the same time, the power size increase accelerated the emptying of the energy storage, thus causing a slight increasing of the LOEP index.

Table 10 reports the results of the simulations performed on the Artemis urban driving cycle. As it can be observed, on a more realistic vehicle speed profile, the e-KERS produced lower recovery efficiencies (from 39% to 48%) but higher energy savings (from 20% to 24%): unlike the previous case, however, increasing the power size produced a beneficial effect on both energetic parameters, which resulted maximized with KERS4. As in the previous case, the LOLP index showed a sharp reduction (from 27% to 4%) with power size increase, while LOEP index revealed again a slight increase (from 15% to 18%).

According to LOEP index results, the storage system can be considered adequately sized for urban application, being its capacity sufficient to exchange the most part of the required energy during the whole driving cycles. As regards the LOLP index, the simulations revealed that, with a proper sizing, the e-KERS is able to satisfy most of the power demand related to vehicle acceleration or braking. In conclusion, the system proved to have good potential, since considerable recovery efficiencies and energy savings were obtained despite the components selected for the KERS assembly are not optimized for this application. Aiming to exploit the e-KERS on a real urban application, the results obtained with the Artemis urban cycle should be considered: according to these simulations, the best configuration for the considered vehicle is the KERS3, equipped with the brushless motor characterized by a continuous and peak power of 12 and 30 kW respectively (see Table 5).

For the evaluation of the real fuel economy connected to the use of the KERS proposed, the authors supposed that the ratio between the net and the real energy required to perform the cycle remains unchanged when evaluated with or without the contribution of the KERS: in other words, the authors supposed that the average efficiency of the internal combustion engine computed on the whole driving cycle remains unchanged when introducing the KERS. According to this assumption, the energy savings produced by the KERS with respect to the net energy E_0 can be extended to the real energy consumed on each driving cycle. As an example, the 24% energy saving obtained in the Artemis urban cycle with KERS4 can also be expected concerning the real energy consumption of the vehicle. Moreover, being the real energy consumed by the

Table 8
Principal simulation configuration parameters.

Solver	ode45 (Dormand-Prince)
Solver type	Variable-step
Max step size [s]	0.05
Min step size [s]	Auto
Initial step size [s]	Auto
Relative tolerance	1e-03
Absolute tolerance	Auto
Shape preservation	Disable all
Num. consecutive min steps	1

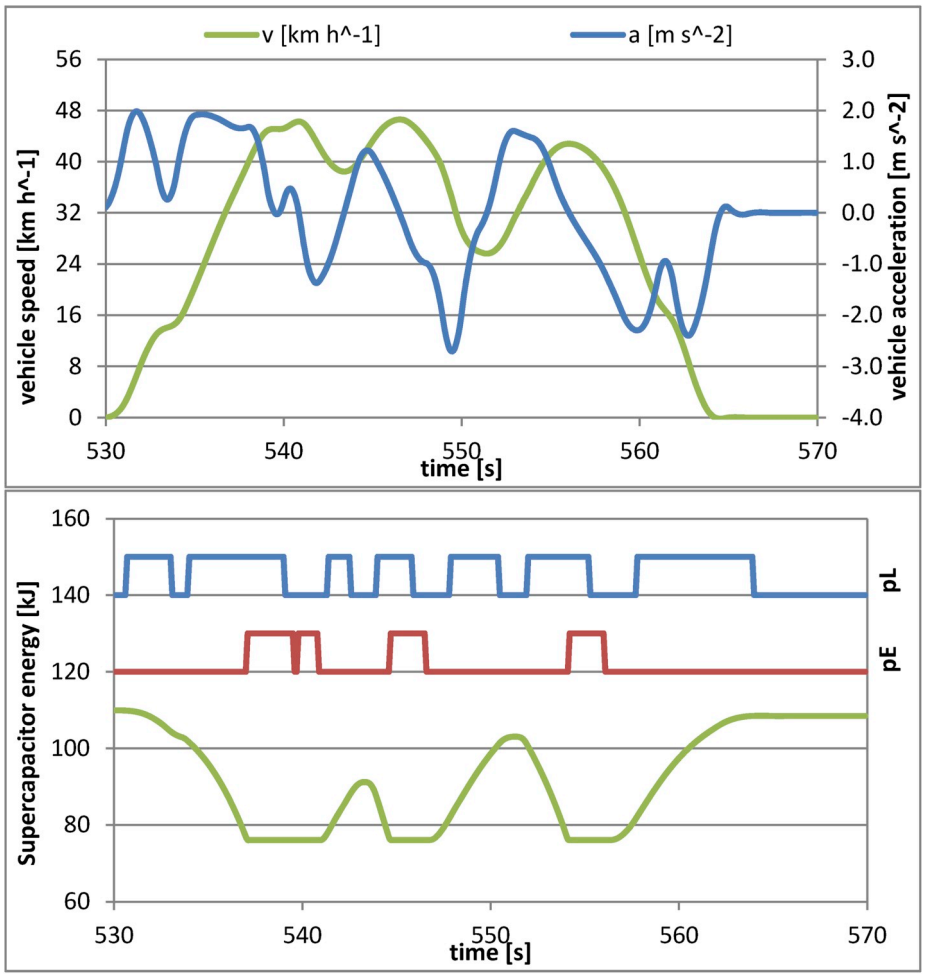

Fig. 6. Upper graph: Vehicle speed and acceleration as function of time; Lower graph: Energy stored in the SC (left axis), Boolean variables p_L and p_E (right axis) as function of time. (Artemis urban cycle, KERS2).

vehicle derived from the fuel combustion, the same energy savings can be applied to the real fuel consumption (reported in Table 2), thus obtaining the fuel savings reported in Table 11 and Table 12 for the two driving cycles ECE-15 and Artemis urban respectively. It is also worth to point out that, since the CO_2 emissions are strictly related to the consumed fuel, the same percentage of fuel savings can be considered valid for the reduction of CO_2 emissions.

The assumption made obviously constitutes a simplified approach, which should be verified. Two considerations, however, can be made in support of this assumption:

(1) Due to air/fuel mixture formation phenomena, the spark ignition engine efficiency during an acceleration transient may result lower with respect to the steady-state operation at the end of the acceleration;
(2) As assumed by the authors, the proposed KERS contributes to vehicle acceleration, thus reducing the participation of the internal combustion engine to this lower efficiency phase, moving hence the most of the thermal engine application to the steady state operations, characterized by higher efficiency.

This means that the assumption made by the authors may also reveal conservative, and the ratio between the net and real energy (i.e. the average engine efficiency) could even be increased by the use of the KERS, producing, as a result, a higher fuel saving than what has been estimated.

Considering the mean European gasoline price of 1.476 € L^{-1}, obtained by the European Environment Agency [16], the estimated fuel savings were converted in the corresponding money savings, as shown in Tables 11 and 12. With the aim to make a comparison with the investment required by the KERS implementation, the estimated money savings were employed to evaluate the probable KERS payback distance, that is the distance that the vehicle has to cover before amortizing the cost of the KERS (reported in Table 7 for each power size). The results of this evaluation are reported in Tables 11 and 12 as well: as it can be observed, the lower payback distances resulted in being about 50,000 km, which, for an average covered distance of 10,000 km $year^{-1}$, may correspond to a payback period of about 5 years. The sense of this evaluation is that the implementation of the KERS proposed could produce such an economic benefit that, after a covered distance of about 50,000 km, the entire system cost would be balanced. From a financial point of view, the best configurations for a real urban application revealed to be KERS1 and KERS2. To further point out the potential of the KERS studied, the authors also evaluated the allowable reduction of CO_2 emissions. As can be observed in the last row of both Tables 11 and 12, for the considered vehicle, the CO_2 emissions that could be avoided (after 100,000 km) by the implementation of the KERS proposed ranges between 16 and 20 tons.

5. Sensitivity analysis

The waveforms reported in Fig. 7 allow to point out that in the system proposed, both the supercapacitor and the MGU can cause insufficient power delivery (as described by the model equations (27) and

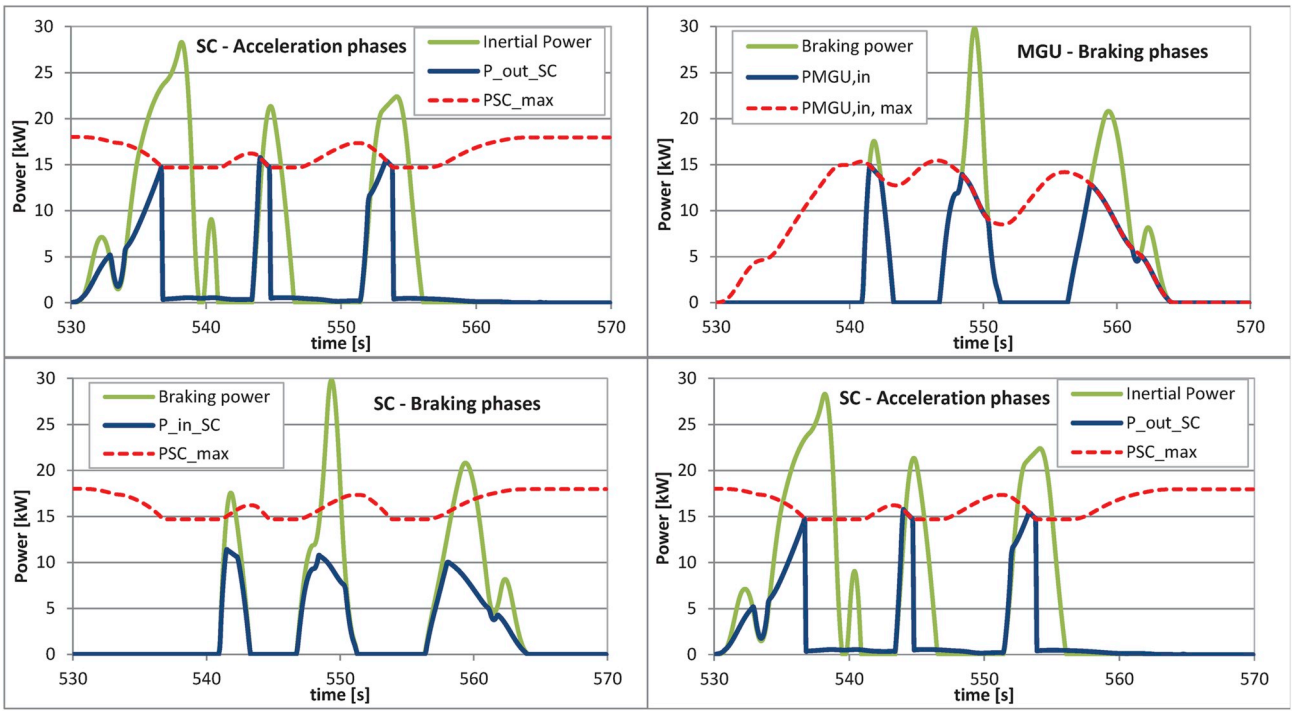

Fig. 7. Upper graph: inertial power, actual and maximum MGU output power as function of time; Lower graph: braking power, actual and maximum MGU input power. (Artemis urban cycle, KERS2).

(47)): as a matter of fact, the power availability of the SC, which reduces when the energy stored decreases, or the power capability of the MGU, which instead is limited by its stall torque or by its maximum allowed peak current, may substantially limit or reduce the effectiveness of the KERS. With the aim to examine the effect of each single element of the KERS on the overall performances, a proper sensitivity analysis was carried out. The purpose of this analysis is to ascertain how limitations and inefficiencies of every KERS component affect the performance parameters (recovery efficiency and energy saving) and the performance indexes (LOEP and LOLP).

The limitations taken into account are:

(1) the power limits imposed by the MGU, reported in the model equations (23), (24) and (27) for the acceleration phase, and in the model equations (45), (46) and (47) for the braking phase.
(2) the power limits imposed by the SC, as reported in the model equations (35) and (37), valid for both acceleration and braking phases.
(3) the limited amount of energy storable, which may prevent the SC to supply the MGU, as described in the model equations (38) and (39), or to recover energy, as described in the model equations (55) and (56).

The inefficiencies considered regards all the three elements of the KERS, i.e.:

(1) the SC, whose efficiency has been described by model equation (33)
(2) the MGU, whose main losses have been described in the model equation (18) (Part 1 of this paper) for the acceleration case, and in the model equation (41) for the braking phase
(3) the power converter, whose efficiency has been expressed by model equations (30) and (31), as function of output and input power respectively.

The analysis carried out by the authors followed the classical *one-at-a-time* procedure, starting from the ideal version of the KERS and gradually introducing the limitation or the inefficiency of each element one at a time (the power size of KERS2 was selected for this analysis). Eight different versions of the KERS were hence obtained, named with capital letters from A to H, reported in Table 13 together with the simulation results obtained on the Artemis urban driving cycle:

- **Version A**: totally ideal KERS, without any power limit, without energy storage limit, and with all efficiencies = 1
- **Version B**: like version A but with limited power and energy storage of the supercapacitor
- **Version C**: like version A but with limited power of the brushless machine
- **Version D**: all power and storage limitations taken into account, all efficiencies = 1
- **Version E**: like version D, considering the real power converter efficiency
- **Version F**: like version D, considering the real MGU efficiency
- **Version G**: like version D, considering the real SC efficiency
- **Version H**: real KERS, with all power and storage limitations, and with all real efficiencies (KERS2)

As mentioned before, each simulation was iteratively repeated until convergence of the initial and final energy in the storage system. The first interesting result is revealed by the totally ideal KERS (version A), which, despite the recovery efficiency of 93% (as expected, the efficiency of both final drive and MGU gear forbid to reach 100%), exhibits an energy saving of 50%, which should be hence considered the reference limit, the asymptote to aim for, and obviously depends on both the driving cycle and the vehicle considered: in other words, for the vehicle adopted, in the Artemis urban cycle the maximum recoverable braking energy amounts to 50% of the net energy required to perform the whole cycle.

Taking into account the SC limitations (in terms of both storage capacity and power limit, KERS version B) led to roughly a 6% reduction on both recovery efficiency and energy saving; considering, instead,

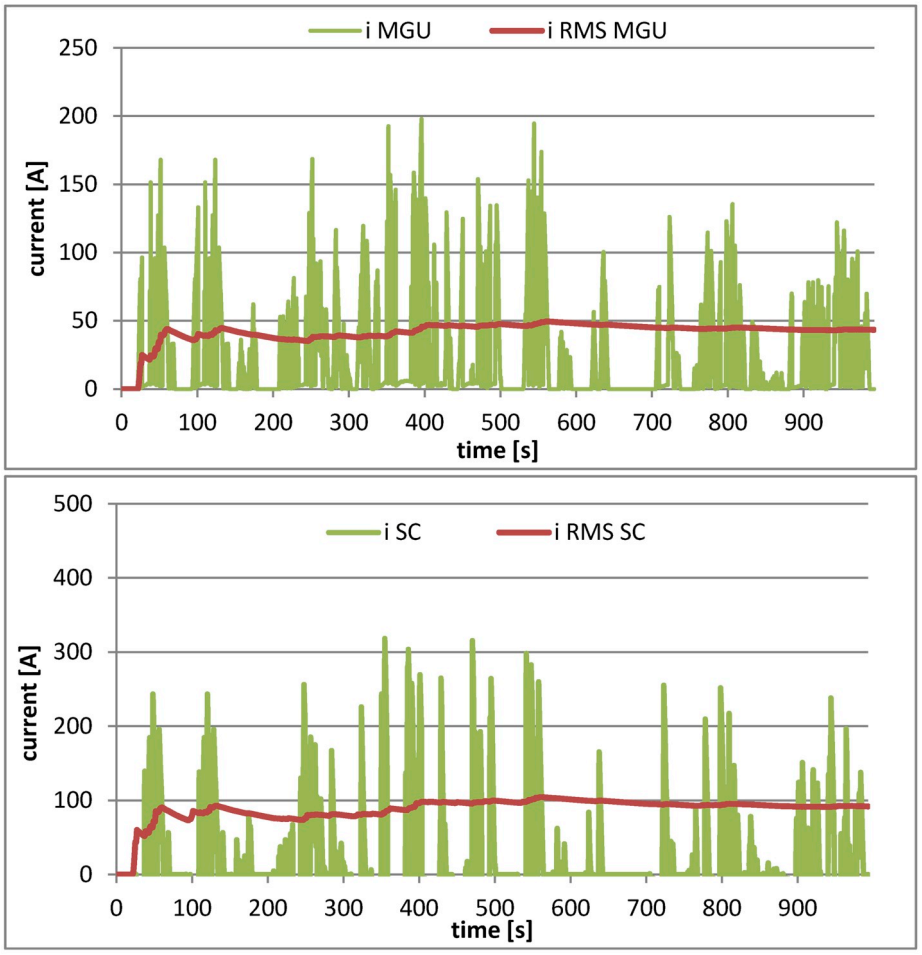

Fig. 8. Upper graph: brushless machine absolute instantaneous and RMS current; Lower graph: supercapacitor absolute instantaneous and RMS current (Artemis urban cycle, KERS2).

Table 9
Results obtained by simulations performed on ECE-15 driving cycle.

	KERS1	KERS2	KERS3	KERS4
Peak motor power [kW]	11.0	14.0	24.0	30.0
Energy required without KERS [kJ]	398	398	398	398
Energy required with KERS [kJ]	323	324	329	334
Recovered energy [MJ]	82.8	81.8	79.4	74.1
Max recoverable energy [MJ]	152	152	153	154
Energy recovery efficiency	54.4%	53.7%	51.8%	48.2%
Energy saving	19.0%	18.7%	17.5%	16.0%
LOEP	8.33%	8.57%	8.95%	9.34%
LOLP	11.9%	3.13%	0.00%	0.00%

Table 10
Results obtained by simulations performed on Artemis urban driving cycle.

	KERS1	KERS2	KERS3	KERS4
Peak motor power [kW]	11.0	14.0	24.0	30.0
Energy required without KERS [kJ]	3006	3006	3006	3006
Energy required with KERS [kJ]	2415	2389	2293	2283
Recovered energy [MJ]	649.1	676.3	791.5	806.2
Max recoverable energy [MJ]	1673	1674	1686	1688
Energy recovery efficiency	38.8%	40.4%	46.9%	47.7%
Energy saving	19.7%	20.5%	23.7%	24.1%
LOEP	15.3%	15.7%	16.8%	17.7%
LOLP	26.7%	22.5%	7.99%	3.96%

Table 11
Estimated fuel economy obtained by the e-KERS (ECE-15 driving cycle).

	KERS1	KERS2	KERS3	KERS4
Fuel consumption with KERS [L $(100\,km)^{-1}$]	6.72	6.75	6.85	6.97
Fuel saving with KERS [L $(100\,km)^{-1}$]	1.58	1.55	1.45	1.33
Money saving with KERS [€ $(100\,km)^{-1}$]	2.33	2.29	2.14	1.96
KERS payback distance [km]	63990	70588	100326	125482
KERS payback time [year]	6.40	7.06	10.03	12.55
CO_2 emissions avoided [ton $(10^5\,km)^{-1}$]	15.6	15.7	15.9	16.2

only the MGU power limits (KERS version C), led to a 23% reduction of recovery efficiency and energy saving with respect to version A: this means that, in the system proposed, the power limits of the MGU resulted in having an effect substantially higher than the limitations introduced by the SC. As a confirmation, when simultaneously considering the limitations of both the MGU and the SC (i.e. KERS version D),

Table 12
Estimated fuel economy obtained by the e-KERS (Artemis urban driving cycle).

	KERS1	KERS2	KERS3	KERS4
Fuel consumption with KERS [L $(100\,km)^{-1}$]	8.27	8.19	7.86	7.82
Fuel saving with KERS [L $(100\,km)^{-1}$]	2.03	2.11	2.44	2.48
Money saving with KERS [€ $(100\,km)^{-1}$]	2.99	3.12	3.60	3.66
KERS payback distance [km]	49750	51764	59529	67227
KERS payback time [year]	4.97	5.18	5.95	6.72
CO_2 emissions avoided [ton $(10^5\,km)^{-1}$]	19.2	19.0	18.3	18.2

Table 13
Sensitivity analysis results (Artemis urban cycle).

	A	B	C	D	E	F	G	H
MGU Power	**100x**	**100x**	**Real**	**Real**	**Real**	**Real**	**Real**	**Real**
SC Storable Energy	**100x**	**Real**	**100x**	**Real**	**Real**	**Real**	**Real**	**Real**
SC Power	**100x**	**Real**	**100x**	**Real**	**Real**	**Real**	**Real**	**Real**
PC efficiency	**1**	**1**	**1**	**1**	**Real**	**1**	**1**	**Real**
MGU efficiency	**1**	**1**	**1**	**1**	**1**	**Real**	**1**	**Real**
SC efficiency	**1**	**1**	**1**	**1**	**1**	**1**	**Real**	**Real**
Recovery efficiency η_K	93.0%	87.2%	72.1%	72.1%	61.8%	52.3%	67.6%	40.4%
Energy saving ε_K	49.8%	46.6%	38.2%	38.2%	32.5%	27.1%	35.7%	20.5%
LOEP	9.74%	9.94%	8.46%	8.45%	11.0%	12.9%	9.53%	15.7%
LOLP	0.0%	5.10%	20.8%	20.9%	21.1%	22.1%	20.9%	22.5%

the results remained unchanged with respect to version C. As regards the performance indexes, it can be observed that, when only power limitations were taken into consideration (KERS version from A to D), LOEP index, which is related to energy, remained almost constant (10%–8.5%). The LOLP index confirmed the effects of the power limits introduced by the MGU, increased from 5% to 21% when passing from version B to C or D.

The effect of the real efficiencies of the three KERS components (power converter, brushless machine and supercapacitor) were taken into account one-at-a-time in the KERS version E, F and G respectively, which revealed, with respect to version D, an energy saving reduction (and an almost equal recovering efficiency reduction) of 14%, 29% and 6%: as it can be deduced, hence, the efficiency of the supercapacitor caused the lowest performance decrement, while the losses in the MGU and in the power converter produced a stronger effect. When considering the losses of all the KERS components simultaneously (version H), the effectiveness of the KERS resulted reduced by 56% with respect to version D, and by 44% with respect to version A. The energy losses of the KERS components caused a moderate increment of the LOEP index, while the LOLP index remained almost unchanged.

The performed sensitivity analysis allowed to point out the aspect of the KERS elements which should be improved to increase the braking energy recovery. As regards the MGU, its limited power output proved to be the major cause of KERS effectiveness reduction: an optimized design should hence maximize both stall torque and peak power, being the continuous power operation less critical. The losses in the power converter revealed to be the second cause of KERS effectiveness reduction: higher conversion efficiencies (up to 0.97) could be achieved by a suitable choice of the power devices and optimizing the layout [17]. As regards the supercapacitor, the adoption of a minimum energy level $E_{SC,min}$ of 40% with respect to rated capacity, allowed to maintain the working voltage $V_{SC}(t)$ sufficiently high to ensure adequate power availability and to restrain the current and the associated ohmic losses.

6. Conclusions

In this two-part paper, the authors propose and evaluate the performance attainable by an electric KERS for internal combustion engine vehicle. The system, as detailed described in the Part 1, was conceived to recover the vehicle kinetic energy during braking phases, to be re-used in successive vehicle acceleration phases. In this way, it is possible to reduce the power demand to the internal combustion engine, and, as a consequence, the related fuel consumption and pollutant emissions. The overall design of the KERS, and hence the selection of its main element, was carried out considering solutions with the minimum increase of the vehicle mass, focusing on market available products, which also allowed to evaluate the related costs. The evaluation of the benefit introduced by the implementation of the KERS proposed was carried through numerical simulation performed with Matlab Simulink, considering the implementation on a widely diffused passenger car (1.4 L spark ignition engine, 90 kW maximum output power, 1315 kg reference mass) and two reference urban driving cycles: the ECE-15 and the more realistic Artemis urban cycle. The sizing of the KERS components, performed through simple energetic evaluation, showed a convergence of the two reference cycles on the energy storage capacity, which, for the vehicle considered, was established to be at least 180 kJ. When focusing on the power size of the KERS, instead, the two cycles exhibited substantial differences, as therefore could be expected, given their different acceleration levels; as a result, 13 kW were found to be sufficient for the ECE-15, while when considering the Artemis urban, the required power size revealed 35 kW: these results led the authors to consider four different KERS assembly (named KERS1, KERS2, KERS3 and KERS4) obtained by combining a single supercapacitor with four brushless motors characterized by different peak power levels (11, 14, 24 and 30 kW respectively), with the aim to identify the optimal choice by means of the numerical simulation. To the purpose, a mathematical model (detailed described in Part 1 of the paper) was realized, taking into account, for each component, the real efficiency and the energy and power constraints introduced in the system. The goodness of the design was assessed by the use of the Loss Of Load Probability (LOLP) and of the Loss Of Energy Probability (LOEP) indexes, while the energetic performances of the KERS were evaluated in terms of energy recovery efficiency (evaluated with respect to the maximum recoverable energy) and energy saving (with respect to the net energy required by the vehicle to complete a whole driving cycle without KERS). According to the results of the simulations performed, the sizing of the energy storage revealed appropriate, as proved by the low values of LOEP obtained (about 8–9% in the ECE-15 driving cycle, and 15–18% in the Artemis urban), which means that the elements of the KERS successfully exchanged almost all the necessary energy. As regards the power size, KERS1 and KERS2, according to the values obtained for the LOLP index (23–27% in the Artemis urban), revealed unsuitable to fulfil the required power transfer between MGU and supercapacitor adequately, while KERS3 and KERS4 revealed appropriate. As concern the energetic performance, the KERS considered in the simulations revealed recovery efficiency in the order of 48–54% for the ECE-15 and 39–48% for the Artemis urban, and energy savings in the range 16–19% for the ECE-15 and 20–24% for the Artemis urban: from a purely energetic point of view, the best choice revealed to be KERS4, which maximized both energy saving and recovery efficiency in the Artemis urban cycle.

Considering that the energy saved corresponds to a reduction of fuel consumption, the authors also evaluated the fuel saving and the related economic advantages (given the average gasoline price in Europe) obtainable by the implementation of the KERS proposed. From an economic point of view, the best configurations for a real urban application revealed to be KERS1 and KERS2: it was estimated that economic benefits gained by their implementation on the selected vehicle could allow balancing their cost within a travelled distance of about 50,000 km. To further point out the potential of the KERS studied, the authors also evaluated the CO_2 emission reduction obtainable: for the vehicle considered, it was estimated that, after 100,000 km, the avoided CO_2 emissions could amount to 19 tons.

The authors consider the results obtained really encouraging, confirming that the managing of the energy during transients by a

supercapacitor based KERS can contribute to the hybridization process of internal combustion engine vehicles and is able to produce an advantage for the customer and for the environment as well.

A sensitivity analysis was also carried out, with the aim to examine the effect of each single element of the KERS on the overall performances: it was understood that, in the system proposed, the power limitations and the losses introduced by the MGU produce the major efficiency penalization with respect to the power converter and to the supercapacitor.

References

[1] E. Pipitone, G. Vitale, A regenerative braking system for internal combustion engine vehicles based on supercapacitors - Part 1: system analysis and modelling, submitted for publication to Journal of Power Sources, available at: http://emilianopipitone.altervista.org/publication_list.htm.

[2] Jisheng Hu, Yukun Zhao, Xiaojing Liu, The design of regeneration braking system in light rail vehicle using energy-storage Ultra-capacitor, in: 2008 IEEE Vehicle Power and Propulsion Conference, Harbin, 2008, pp. 1–5, https://doi.org/10.1109/VPPC.2008.4677708.

[3] M. Ouyang, W. Zhang, E. Wang, F. Yang, J. Li, Z. Li, P. Yu, X. Ye, Performance analysis of a novel coaxial power-split hybrid powertrain using a CNG engine and supercapacitors, Appl. Energy 157 (2015) 595–606, https://doi.org/10.1016/j.apenergy.2014.12.086.

[4] B. Lequesne, Automotive electrification: the nonhybrid story, IEEE Trans. Transp. Electr. 1 (1) (June 2015) 40–53, https://doi.org/10.1109/TTE.2015.2426573.

[5] P. Mock, European Vehicle Market Statistics 2018/2019, International Council on Clean Transportation Europe (ICCT), 2018. www.theicct.org.

[6] C. Vock, J. Hubel, D. Tsokolis, C. Samaras, L. Ntziachristos, R. Tola, C. Ricci, Z. Samaras, Report on the Development and Use of the Vehicle Energy/Emission Simulator, Deliverable D.3.2.1, 2014 (ICT-EMISSIONS Consortium).

[7] T.J. Barlow, S. Latham, I.S. McCrae, P.G. Boulter, A Reference Book of Driving Cycles for Use in the Measurement of Road Vehicle Emissions, 2009. Published project report, ISSN 0968-4093, HIS.

[8] E.G. Giakoumis, Driving and Engine Cycles, Springer International Publishing, 2017. ISBN: 783319490342 978-3-319-49034-2.

[9] M. André, The ARTEMIS European driving cycles for measuring car pollutant emissions, Sci. Total Environ. 334–335 (2004) 73–84, https://doi.org/10.1016/j.scitotenv.2004.04.070.

[10] UNECE, Development of a World-wide Worldwide Harmonized Light Duty Driving Test Cycle (WLTC), 2013. UN/ECE/WP.29/GRPE/WLTP-IG, Technical Report GRPE-68-03.

[11] http://www.greentechee.com/48V-165F-super-capacitor-modules-with-large-power_p41.html.

[12] http://www.evdrives.com/.

[13] http://motenergy.com/brdcmo2.html.

[14] J.W. Dixon, I.A. Leal, Current control strategy for brushless dc motors based on a common DC signal, IEEE Trans. Power Electron. 17 (2) (2002) 232–240, https://doi.org/10.1109/63.988834.

[15] G. Vitale, E. Pipitone, A six legs buck-boost interleaved converter for KERS application, submitted for publication to World Electric Vehicle Journal, currently available for consultation at, http://emilianopipitone.altervista.org/publication_list.htm, 2019.

[16] European environment agency [online], https://www.eea.europa.eu/data-and-maps/indicators/fuel-prices-and-taxes/. (Accessed February 2019).

[17] J. Kolar, F. Krismer, Y. Lobsiger, J. Muhlethaler, T. Nussbaumer, J. Minibock, Extreme efficiency power electronics, in: 7th International Conference on Integrated Power Electronics Systems, 2012, 6185790. CIPS 2012.

Symbols and abbreviations

a, $a(t)$: vehicle acceleration, as function of time t
A_f: frontal area of the vehicle
C: capacitance
CNG: compressed natural gas
CVT: continuous variable transmission
c_r: rolling resistance coefficient
c_x: drag coefficient of the vehicle
E_{br}: energy that can be recovered during a braking phases
E_0: net energy demand to the thermal engine to perform a complete driving cycle without KERS
E_K: net energy demand to the thermal engine to perform a complete driving cycle with KERS
E_{MR}: maximum recoverable energy in a whole driving cycle
E_S: traction energy delivered by the MGU during a driving cycle
E_{SC}: energy stored in the supercapacitor
$E_{SC,max}$: maximum storable energy in the supercapacitor
$E_{SC,min}$: minimum allowed energy content of the supercapacitor
ECE-15: European urban driving cycle
ESR: equivalent series resistance of the supercapacitor
EUDC: European extra urban driving cycle
F_{aer}: vehicle aerodynamic resistance
F_{br}: braking force acting on the vehicle
F_{dist}: external disturbance force acting on the vehicle
F_{grav}: force of gravity acting on the vehicle in the case of a slope
F_{road}: road load (vehicle resistance to the movement)
F_{roll}: vehicle rolling resistance
F_{trac}: traction force acting on the vehicle
I: MGU rotor inertia
i_{MGU}: current on the DC side of the MGU controller
$i_{MGU,\ max}$: maximum allowed current on the DC side of the MGU controller
$i_{MGU,\ SL}$: MGU current limit imposed by the maximum power output of the supercapacitor
$i_{PC,max}$: maximum allowed current in the power converter
i_{SC}: current in the supercapacitor
ICE: internal combustion engine
ICEV: internal combustion engine vehicle
k: windage losses constant of the MGU
KERS: kinetic energy recovery system
L_F: mechanical friction losses of the MGU
L_{MGU}: MGU power losses
L_R: resistive and power interrupter losses of the MGU
L_W: windage losses of the MGU
m_v: vehicle mass
MGU: motor generator unit
$n_{MGU,\ max}$: maximum rotation speed of the MGU
NEDC: new European driving cycle
p: tires pressure
P_{br}: braking power
p_E: loss of energy Boolean variable
P_{eng}: power output from the internal combustion engine
P_I: inertial power
p_L: loss of power Boolean variable
P_{MGU}: power output from the MGU
$P_{MGU,max}$: maximum power output from the MGU
$P_{MGU,in}$: power input to the MGU
$P_{MGU,in,max}$: maximum power input to the MGU
P_{PC}: power output from the power converter
$P_{PC,max}$: maximum power output from the power converter
$P_{PC,in}$: power input to the power converter
$P_{PC,in,max}$: maximum power input to the power converter
P_{road}: road load power
P_{SC}: power output from the supercapacitor
$P_{SC,in}$: power input to the supercapacitor
$P_{SC,max}$: maximum power output from the supercapacitor
P_{trac}: traction power acting on the vehicle
PC: power converter
PMSM: permanent magnet synchronous motor
R: the resistive losses constant of the MGU
RMS: root mean square value
R_W: vehicle wheel radius
SC: supercapacitor
UDC: urban driving cycle
t: time
T_F: constant friction torque of the MGU
T_{MGU}: torque delivered by the MGU
$T_{MGU,max}$: maximum torque that the MGU can deliver (as motor) or receive a(as generator)
$T_{MGU,\ CL}$: MGU torque limit imposed by the maximum allowed current $i_{MGU,max}$
$T_{MGU,\ SL}$: MGU torque limit imposed by the maximum power output of the supercapacitor
$T_{MGU,\ stall}$: peak stall torque of the MGU
v, $v(t)$: vehicle speed, as function of time t
V_{MGU}: voltage on the DC side of the MGU controller
$V_{MGU,\ max}$: maximum allowed voltage on the DC side of the MGU controller
V_{SC}: instantaneous working voltage of the supercapacitor
$V_{SC,\ max}$: maximum allowed voltage of the supercapacitor
WLTC: worldwide harmonized light vehicles test cycles
x_{PC}: normalized output power from the power converter
$x_{PC,in}$: normalized input power to the power converter
$\alpha(t)$: MGU angular acceleration (function of time)
δ_a: air density
η_D: efficiency of the final differential gear
η_G: efficiency of the gear between MGU and drive shaft
η_{MGU}: MGU efficiency
η_{PC}: power converter efficiency
η_{PC}^*: power converter efficiency at its maximum output power
η_{SC}: supercapacitor efficiency
η_T: efficiency of the vehicle main transmission
τ_D: differential gear ratio
τ_G: MGU gear ratio
$\omega(t)$: MGU rotational speed (function of time)